J. Am. Soc. Mass Spectrom. (2017) 28:1575–1586
DOI: 10.1007/s13361-017-1640-0

RESEARCH ARTICLE

Influence of Ionization Source Conditions on the Gas-Phase Protomer Distribution of Anilinium and Related Cations

Athula B. Attygalle, Hanxue Xia, Julius Pavlov

Center for Mass Spectrometry, Department of Biomedical Engineering, Chemistry, and Biological Sciences, Stevens Institute of Technology, Hoboken, NJ 07030, USA

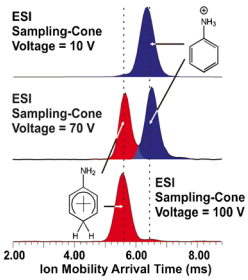

Abstract. The gas-phase-ion generation technique and specific ion-source settings of a mass spectrometer influence heavily the protonation processes of molecules and the abundance ratio of the generated protomers. Hitherto that has been attributed primarily to the nature of the solvent and the pH. By utilizing electrospray ionization and ion-mobility mass spectrometry (IM-MS), we demonstrate, even in the seemingly trivial case of protonated aniline, that the protomer ratio strongly depends on the source conditions. Under low in-source ion activation, nearly 100% of the *N*-protomer of aniline is produced, and it can be subsequently converted to the *C*-protomer by collisional activation effected by increasing the electrical potential difference between the entrance and exit orifices of the first vacuum region. This activation and transformation process takes place even before the ion is mass-selected and subjected to IM separation. Despite the apparent simplicity of the problem, the preferred protonation site of aniline in the gas phase—the amino group or the aromatic ring—has been a topic of controversy. Our results not only provide unambiguous evidence that ring- and nitrogen-protonated aniline can coexist and be interconverted in the gas phase, but also that the ratio of the protomers depends on the internal energy of the original ion. There are many dynamic ion-transformation and fragmentation processes that take place in the different physical compartments of a Synapt G2 HDMS instrument. Such processes can dramatically change the very identity even of small ions, and therefore should be taken into account when interpreting product-ion mass spectra.

Keywords: Protomers, Anilinium ion, Protonated aniline, Ion mobility, Tautomerization

Received: 22 November 2016/Revised: 23 February 2017/Accepted: 25 February 2017/Published Online: 10 April 2017

Introduction

The question of protonation sites of gas-phase aromatic compounds has been the subject of extensive studies [1–12]. For many mass spectrometric (MS) investigations, protonated gas-phase molecules are generated under ambient conditions by electrospray (ESI), atmospheric-pressure, or in vacuo chemical and plasma ionization processes [13]. In the process of ionization, the charge-imparting proton can sometimes attach to different sites, thus forming a mixture of several isomeric tautomers [9, 14]. We prefer to designate such prototropic isomers as protomers, with the caveat that the term has been used previously in the entirely different context of structural biology to name distinct protein chains that form a larger hetero-oligomer [15].

Many previous investigations have addressed whether the protonation regio-selectivity of a given gaseous molecule formed from sprayed droplets directly reflects the situation in the original bulk liquid; however, the subject remains highly debatable [16–21]. Generally, the preferred protonation site of a polyfunctional molecule can be predicted by computational methods [19]. Nevertheless, even for a simple molecule such as aniline, theoretical studies can often be inconclusive in predicting an unequivocal protonation site [22–27]. In computational studies, the final predictions are strongly dependent on the levels of theory and the basis sets of functions employed [25, 28]. It has been noted that some protonated species formed under certain MS ionization conditions are not always the thermodynamically most favored species [18]. This is not unexpected because usually species investigated under MS

Electronic supplementary material The online version of this article (doi:10.1007/s13361-017-1640-0) contains supplementary material, which is available to authorized users.

Correspondence to: Athula Attygalle; *e-mail:* athula.attygalle@stevens.edu

conditions are not in their lowest energy states. Sometimes, kinetically controlled protonation could take place at a less preferred site due to steric, thermal, or other factors [18–21, 29, 30]. Whatever the case may be, different protomers of the same molecule can undoubtedly coexist in the gas phase [9].

Based on results from a gas-phase ion-molecule reaction with pyridine, Smith et al. [8] found that nearly 90% aniline molecules under certain experimental conditions were protonated on the nitrogen atom, and concluded that this is the kinetically favored protonation site. Similarly, the preferred generation of *N*-protonated aniline has been reported under ammonia-chemical ionization of chlorobenzene [31]. Flammang et al. also observed that *N*-protonated aniline is the major isomer produced in the gas phase; however, they indicated that post-ionization collisional isomerization may take place between the *N*- and *C*-protomers (Scheme 1) [28].

Although not much attention has been paid to post-ionization isomerization processes that could take place upon collisional activation of mass-selected ions, as early as 1993 Bakhtiar et al reported that the $Si(C_2H_5)H_2^+$ ion could isomerize to $Si(CH_3)_2H^+$ upon collisional activation [32].

Extensive experimental and theoretical studies have been carried out to determine the factors influencing the abundance ratio of protomers formed during positive-ion-generating ESI [33]. The general consensus is that the protic or aprotic nature of the solvent, the ionic strength and pH of the solution, and the solution-based chemical equilibrium that exists between the base and its conjugate acid determine the manifested protomer ratio [34]. On the other hand, the existence of protomers has been noted even under atmospheric-pressure chemical ionization (APCI) conditions [18]. Because analytes are often sprayed as solutions, the nature of the solvent has been regarded as the major factor that controls the ratio of protomers, even under APCI conditions.

For tandem MS, ions generated in an ion source are often isolated by a quadrupole filter and transferred to a collision cell, where they are subjected to collision-induced dissociation (CID). In a Synapt G2 HDMS instrument, an ion mass-selected by the quadrupole analyzer is transferred to a Triwave cell consisting of three traveling-wave assemblies. Ions are briefly accumulated in the Trap region, and released to a traveling-wave ion-mobility (TWIM) cell via a chamber filled with helium (Supplementary Figure S1) [35]. Ions separated by IM then pass a Transfer cell and undergo acceleration by the pusher before they are mass-separated by the time-of-flight (ToF) analyzer. A product-ion mass spectrum can be generated by subjecting an ion to CID either in the Trap or the Transfer region. Generally, when MS fragmentation experiments are conducted, the experimental conditions that are primarily tuned are the collision-cell parameters. Customarily, when ion-fragmentation pathways are deliberated, one specific structure is selected to represent the precursor ion. The selected structure is generally the lowest-energy configuration predicted by computational methods. Although it is well known that ions undergo activation and fragmentation while being transferred from the atmospheric-pressure source area to the high-vacuum analyzer region [36], the possibility that ions could also experience conformational or structural isomerization *during this transfer process* has not been sufficiently appreciated. Such transformations occur particularly in the first low-vacuum region of a mass spectrometer (Supplementary Figure S1). If isomerizations occur prior to the ion isolation and CID, the strong possibility exists that the precursor ion can be represented by several distinct structures. In other words, a CID spectrum recorded in this way may well be that of a *composite* from several isomeric precursor ions.

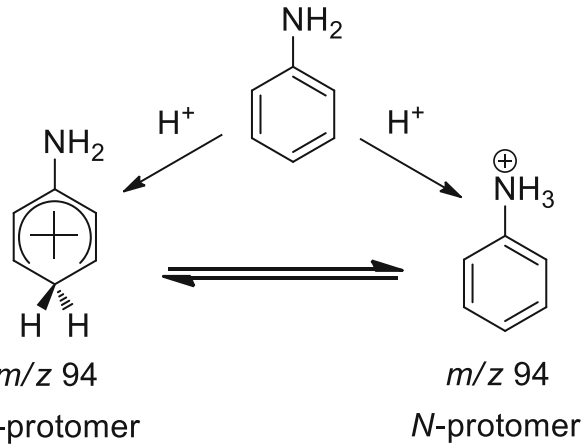

Scheme 1. Protonation of aniline to afford either *N*-protonated or *ring*-protonated (*C*-protonated) species

There have been many attempts to design artificial intelligence (AI) programs to automate the interpretation of CID spectra in order to identify compounds [37, 38]. However, if the definitive structure of the precursor ion is uncertain, many spectra currently compiled in databases could well be regarded as composites representing mixtures of protomers (or deprotomers). In this respect, AI programs currently available for the interpretation of CID spectra are clearly inadequate for the unambiguous identification of compounds.

Révész et al. have noted that diastereomeric interconversion of some Tröger bases can be caused by activation in the in the ESI ion source [39]. We recently reported that negative-ion-generating ESI source conditions exert a dramatic effect on the tautomer distribution of deprotonated *p*-hydroxybenzoic acid in the gas phase [40]. Herein, we report a similar effect on the abundance ratio of the protomers derived from aniline and related compounds under positive-ion ESI-MS.

Experimental

Materials

All chemicals, including aniline, *p*-toluidine, *p*-aminophenol, and *p*-fluoroaniline were purchased from Sigma-Aldrich Chemical Co. (St. Louis, MO, USA) and used without further purification. Ultrapure water was obtained from a Milli-Q purification system (Millipore Corporation, Bedford, MA,

USA). All test solutions (50 ppm) were prepared in 50:50 v/v acetonitrile:water containing 1% formic acid.

Mass Spectrometry

Spectra were acquired on a Synapt G2 HDMS instrument (Waters, Milford, MA, USA) equipped with an ESI, an ASAP, or a HePI source. For ion-mobility (IM) experiments, the ions of interest were mass-selected and transferred to the Triwave cell, where they were briefly accumulated in the Trap region, and released to the TWIM cell [34]. After the IM separation, the ions passed through the Transfer cell and underwent acceleration by the pusher before they were mass-separated by the time-of-flight analyzer. Unless otherwise specified, all IM separation experiments were carried out under the following typical instrumental conditions: Trap collision energy 4 eV, Transfer collision energy 2 eV, IM wave velocity 1500 m/s, IM wave height 40.0 V, scroll-pump pressure 3.13 mbar, source pressure 1.36×10^{-3} mbar, helium-cell pressure >14.1 mbar, IM-cell pressure 4.45 mbar (N_2), TOF analyzer pressure 9.68×10^{-7} mbar, Trap pressure 4.49×10^{-2} mbar (Ar), and Transfer pressure 4.87×10^{-2} mbar (Ar).

The general source conditions for electrospray-ionization (ESI) experiments were as follows: capillary voltage 2.55 kV, extraction cone 3.0 V, desolvation-gas flow rate 477 L/h, sample infusion flow rate 15 μL/min, and Vernier-probe-adjuster position 5.92 mm. The source- and desolvation-gas temperatures were held at 80 and 100 °C, respectively. To investigate individual effects, the magnitude of the sampling-cone voltage was varied between 10 and 70 V while other parameters were kept constant.

For the ASAP-APCI experiment, a glass tube smeared with aniline was inserted to the probe. Spectra were recorded under the following conditions: corona voltage 5.0 kV, extraction cone 3.0 V, desolvation-gas flow rate 477 L/h, Vernier-probe-adjuster position 5.92 mm, probe temperature 100 °C, source 80 °C, and desolvation-gas temperature 100 °C.

For helium-plasma ionization (HePI) [41], a stream of high-purity helium at a flow rate of about 30 mL/min was passed through a stainless steel capillary needle (100 μm i.d.) held at an electrical potential of +3.67 kV. Other instrument parameters for the HePI experiment were as follows: extraction cone 3.0 V, desolvation-gas flow rate 477 L/h, and Vernier-probe-adjuster position 5.92 mm. The source- and desolvation-gas temperatures were held at 80 and 100 °C, respectively. To investigate sampling-cone activation effects, the voltage was varied between 10 and 120 V while other parameters were kept constant. For atmospheric-pressure ion generation, a few milligrams of pure sample in a 2 mL vial was placed near the cone entrance and the capillary tip within the ion-source chamber.

Computational Methods

All calculations were done using Gaussian 09 [42]. Geometries for all species proposed for the fragmentation pathways were fully optimized by the B3LYP [43] method (Becke's three-parameter nonlocal-exchange functional with the nonlocal correlation functional of Lee et al. [44]), using a large 6-311++G(2d,2p) basis set. Frequency calculations were performed at the same level to verify the nature of each stationary state on the potential-energy surface. Reactants/products were associated with all positive vibrational frequencies, and transition states (TS) were associated with only one imaginary frequency, for which the normal vibrational mode corresponded to the expected bond formation/breaking movements in a specific reaction pathway. Gibbs free energies were calculated for room temperature and ambient-pressure conditions.

Results and Discussion

For ESI-MS analysis, gaseous ions generated under atmospheric-pressure ESI conditions are transferred through several modular units of independently pumped physical compartments maintained under different vacuum conditions, after which the ions are subjected to mass analysis in the high-vacuum region. The first low-vacuum compartment, immediately after the atmospheric-pressure section, has an entrance nozzle (sampling cone entrance) and an exit orifice (extraction cone) (Supplementary Figure S1). An electrical potential difference is maintained between these two orifices to increase the ion transmission efficiency (often called the *sampling-cone voltage*) [36]. It is known that in addition to increased transfer efficiency, the ions gain acceleration and endure vibrational activation due to collisions between themselves and the residual gaseous molecules in this region [36, 45–47].

We generated gaseous protonated aniline (*m/z* 94) by electrospraying an acidified acetonitrile-water solution of aniline. The ions were then mass-selected by the quadrupole analyzer and transferred to the traveling-wave ion-mobility (TWIM) cell for separation, and an arrival-time distribution (ARD) profile was recorded. As in results reported by Lalli et al. [48], we observed two peaks with different arrival times for the *C*-protonated and *N*-protonated aniline species upon IM separation of the *m/z* 94 ion (Figure 1b). The more mobile, first-to-arrive protomer has been identified as the *C*-protonated species (although this ion is referred to as the *C*-protomer in the literature, it represents the species protonated at the *para*–ring position; Scheme 1) [48]. Moreover, the 1:5 area ratio observed by Lalli et al. for the two peaks was suggested to represent the intrinsic proportion of the two aniline protomers in the gas phase because the IM profile did not change when a methanolic solution was sampled at different pHs [48].

However, we noticed that the ratio of the two species is highly dependent on the ion-source parameters. In particular, the sampling-cone voltage exerts a profound influence on the protomer ratio. For example, the ATD recorded from the *m/z* 94 ion generated at a sampling-cone voltage setting of 10 V showed essentially one peak – for the second-to-arrive *N*-protomer (Figure 1a). Upon gradual increase of the sampling-cone voltage, a dramatic increase of the abundance of the first-to-arrive ion was observed. In fact, our cone-voltage-

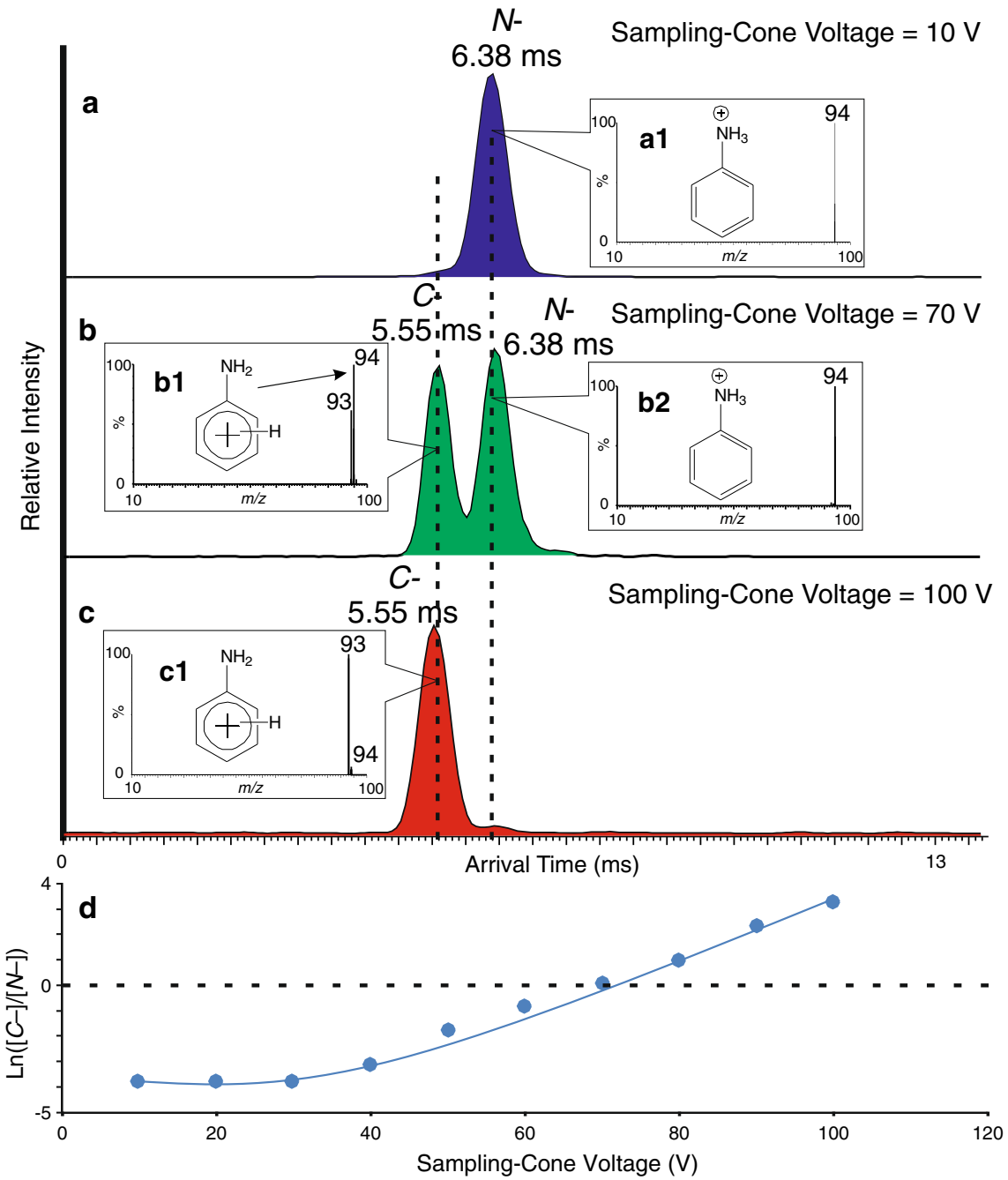

Figure 1. Arrival-time distributions (ATDs) recorded from IM-separated mass-selected *m/z* 94 ion generated by ESI from aniline, in 50:50 acetonitrile:water containing 1% formic acid, at sampling-cone voltages of 10 (**a**), 70 (**b**), and 100 V (**c**). IM separation was carried out at a wave velocity of 1500 m/s and a wave height 40.0 V. Other experimental parameters were: Vernier-probe-adjuster setting 5.92 mm, capillary voltage 2.55 kV, extraction cone 3.0 V, desolvation-gas flow rate 477 L/h, source temperature 80 °C, desolvation-gas temperature 100 °C, trap collision energy 4 eV, and transfer collision energy 2 eV. Insets depict CID spectra corresponding to peaks in the ATD. Panel (**d**) shows a plot of the natural logarithm of *C*-/*N*- peak ratios extracted from ATDs recorded at different sampling-cone voltage settings

varying experiments showed that the *N*-protomer is the dominant species when the cone-voltage difference is relatively low (<30 V) (Figure 1d). However, as the cone voltage was gradually raised, the formation of the *C*-protomer became more favored. At a setting of 70 V, we observed a ratio of 1:1.1. At about 100 V, the only peak in the arrival-time profile was that at 5.55 ms (Figure 1c). Since the abundance of the *C*-protomer observed at lower voltages is much lower than that in the ratio reported by Lalli et al. [48], it is evident that the 1:5 ratio should not be considered as either intrinsic or constant for the aniline protomers. We propose that the *N*-protomer undergoes a conversion to the *C*-protomer in the supersonic expansion region due to post-ionization collisional isomerization.

Previously, Kaufmann et al. [33] reported that the IM arrival-time profiles of protomers of norfloxacin change when the cone-voltage settings were varied from low to high values. However, such changes had been attributed to differences in the fragmentation rates of the individual protomers.

Although not as dramatic as that instigated by the sampling-cone voltage, a similar change in the protomer ratio was also noted when the extraction-cone voltage was increased (Supplementary Figure S2). This less significant effect was understandable because far fewer neutral molecules, needed for collisional activation, make their way through the extraction-cone (skimmer) orifice.

As mentioned above, the *N*-protomer is the predominant species in the gas phase when aniline is subjected to electrospray ionization at lower cone voltages (<30 V). Interestingly, even under <30 V sampling-cone-voltage conditions, a significant formation of the *C*-protomer was witnessed when aniline was ionized by more energetic ion-generation methods such as the ambient solids analysis probe (ASAP) [49], CI, APCI, or helium-plasma ionization (HePI) [40] (Figure 2). In other words, the observed ratios of the protomers depend on the *internal energy* of the precursor ion (often referred to as the "hotness" of the ion) at the commencement of an ion-mobility separation. For example, the initial *C*-/*N*-protomer ratio generated under HePI conditions at a sampling-cone voltage setting of 30 V is higher than that recorded under ESI conditions. Even the *C*-/*N*-protomer ratio observed under HePI conditions increased dramatically as the cone voltage was raised (Figure 2f).

The existence of differently protonated species originating from the same analyte has been recognized previously [33] in an indirect manner by the qualitative differences observed in the CID spectra recorded for certain isolated ions under identical tandem mass spectrometric conditions, but at low- and high-cone-voltage ion-generation settings. Results from the present study show that the MS^2 spectra recorded for the *m/z* 94 ion from aniline at different sampling-cone voltages but under identical collision-cell conditions (with or without collision gas), differ from each other (Supplementary Figure S3). The spectra recorded for the *m/z* 94 ion generated at high cone voltages (>50 V) showed a fragment ion peak at *m/z* 93 for a $H^{\bullet}$ loss even when no argon was present in in the collision cell. Apparently, the *m/z* 94 ions generated at high sampling-cone voltages (above 50 V) arrive at the collision cell carrying sufficient internal energy to undergo unimolecular dissociation, and generate the *m/z* 93 ion without the need for any further activation in the collision cells (Supplementary Figure S3B). It has been assumed that the gas-phase protomer ratio manifested in the ion source is related to the ion chemistry in solution [10], and the changes in the spectra have been attributed to the differences in the ion fragmentation rates of the protomers [33]. To explain the differences in the spectra recorded without IM separation, we must first rationalize how each protomer fragments. It has been established that the *N*- and *C*-protomers of aniline can be differentiated by their distinctive fragmentation spectra [9, 48]. The *C*-protomer dissociates by a preferential homolytic mechanism to eliminate a $H^{\bullet}$ and generate the molecular ion of aniline (*m/z* 93, Scheme **2**) (Supplementary Figure S4). In contrast, the *N*-protomer fragments by a NH_3 loss to generate the phenyl cation (*m/z* 77, Scheme **2**). The *m/z* 77 ion can be used as a diagnostic marker to recognize the *N*-protomer [28]. However, the formation of the *m/z* 77 ion requires more activation of the precursor than that required

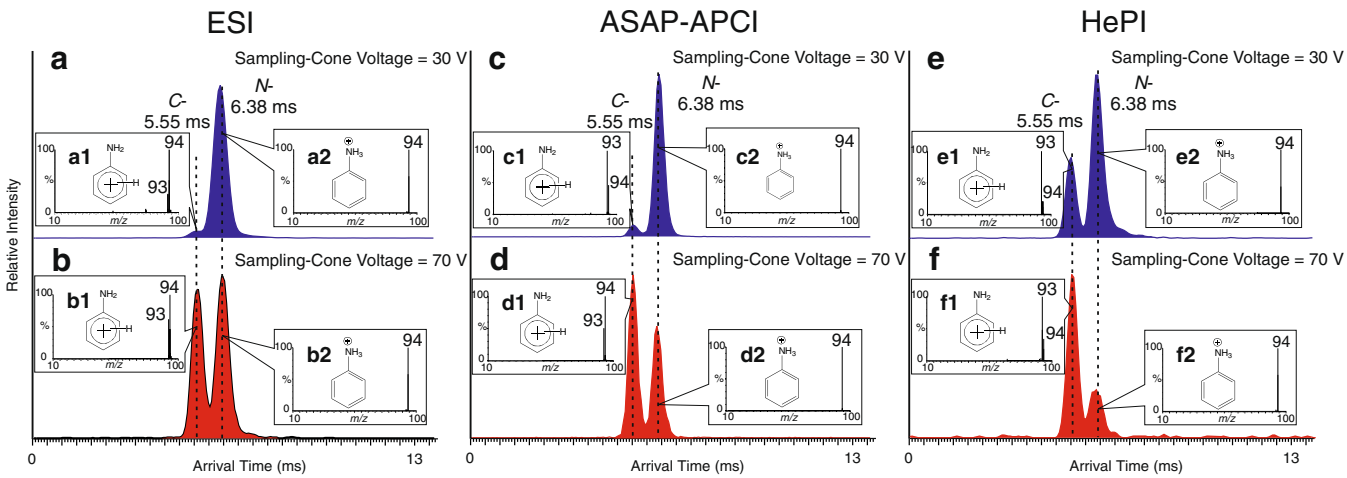

Figure 2. Arrival-time distributions (ATDs) recorded from mass-selected the *m/z* 94 ion generated by ESI (**a** and **b**), ASAP-APCI (**c** and **d**), or HePI (**e** and **f**), from aniline at a sampling-cone voltage settings of 30 V (**a**, **c**, and **e**), or 70 V (**b**, **d**, and **f**). The *m/z* 94 ion was generated by ESI by spraying an aqueous sample of aniline (**a** and **b**) at a capillary voltage of 2.55 kV, or by ASAP-APCI by inserting a glass tube smeared with aniline, at a corona voltage setting at 5.0 kV (**c** and **d**), or by HePI by placing a few milligrams of aniline near the cone entrance and capillary tip within the ion-source chamber, and passing 30 mL/min of helium through the metal capillary tube held at 3.67 kV (**e** and **f**). The other experimental conditions were identical to those given in Figure 1. Insets A1-F1 show CID spectra corresponding to the arrival-time peak at 5.55 ms, and A2-F2 show those corresponding to the 6.38 ms peak recorded at Trap and Transfer collision energy of 4 and 2 eV, respectively

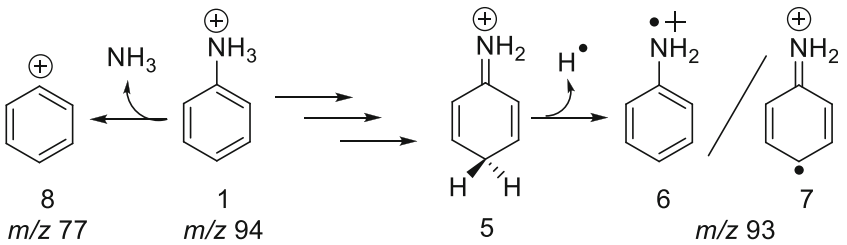

Scheme 2. Proposed fragmentation pathways for protonated aniline

for the *m/z* 93 ion. For example, at a Transfer collision energy of 5 eV, a peak for the *m/z* 77 ion is not observed in the CID spectra of either protomer, whereas a distinct peak is seen at *m/z* 77 when the collision energy is raised to 20 eV (Supplementary Figure S4).

From our observations, it is evident that the dissimilarities in the spectra are primarily attributable to the variations in the protomer abundances brought about by changes in the *source conditions*, rather than by the changes ensuing from differences in *fragmentation rates*. For example, the 5.55 ms arrival-time peak in Figure 1b, which was recorded at a sampling-cone setting of 70 V, represents a composite mixture of both the precursor (*m/z* 94) and its product ions generated by fragmentation (primarily, the *m/z* 93 ion). However, the fragmentation of the precursor, mediated by the sampling-cone voltage, is not the fundamental reason for the changes of the intensity ratios of the IM peaks at 5.55 ms and 6.38 ms. To support this proposition, we extracted absolute signal intensities of the *m/z* 94 ion from the IM profile data recorded from protonated aniline at different sampling-cone voltages (Supplementary Figure S5). Clearly, the intensity of the *m/z* 94 peak at 5.55 ms (Supplementary Figure S5, **B1**-**B10**) increases as the sampling-cone voltage is raised, demonstrating the increasing formation of *C*-protonated aniline as the cone voltage is raised. The peak-intensity increase is evident even if we disregard the contributions due to fragmentation (Supplementary Figure S5, **C1**–**C10**). Intensity profiles normalized to a scale of 100 showed that the intensity of the *m/z* 93 peak can be used as a diagnostic marker for the *C*-protomer (Supplementary Figure S6). Although the fragmentation rates of the two protomers are different (Supplementary Figure S4), it is the tautomerization effected by ion activation in the source that is primarily responsible for the dissimilarities in the overall fragmentation spectra. The *m/z* 93 ion, which originates from the *C*-protomer, can be formed in the Trap or the Transfer region of the Triwave cell by activation of the *m/z* 94 ion (Supplementary Figure S4). An arrival-time profile recorded from the IM-separated mass-selected *m/z* 93 ion ($C_6H_7N^{+\bullet}$, the molecular ion of aniline) generated by HePI at a sampling-cone voltage of 70 V from a sample of aniline placed in the source, showed that $C_6H_7N^{+\bullet}$ ion bears the same mobility as that of the *C*-protomer (Supplementary Figure S7); in fact, the 20 eV Transfer-cell fragmentation spectrum was comparable to the electron-ionization library spectrum of aniline. Thus, if the *m/z* 93 ion is generated in the trap region from the *C*-protomer, it will co-elute with the *m/z* 94 ion of the undissociated *C*-protomer, thereby generating a composite mobility peak (Figure 1b).

The induced in-source formation of *C*-protonated aniline can also be indirectly demonstrated even without the need of an IM separation: with increasing sampling-cone voltage, the abundance of the *C*-protomer-specific fragment-ion at *m/z* 93 shows an upward trend even when the empty Triwave cell is operated simply as a transfer line (Supplementary Figure S3). The *m/z* 94 ions generated at high sampling-cone voltages and isolated by the quadrupole analyzer arrive sufficiently activated, and undergo unimolecular fragmentations, even when there is no argon in the Trap and Transfer collision cells (Supplementary Figure S3, Panel B7).

Although our experimental results indicated that the *N*-protonation in aniline is kinetically preferred, ab initio calculations performed at the B3LYP/6-311++G(2d,2p) level of theory indicated that the *para*-ring carbon is the energetically favored protonation site; however, the calculated energy difference between the two species is only 2.19 kcal/mol (Figure 3a) [8]. Moreover, certain calculations conducted at higher levels of theory suggest that the most favored protonation site is the *para*-ring position, but lower-level computations suggest the opposite result [25]. Evidently, the total energy calculations for protonated aniline are highly sensitive to the selected theoretical method [25]. Thus, it is difficult to assign a reliable global-energy-minimum structure by computational methods [25, 28]. In other words, it is quite possible that the *N*-protonated species is the true global-minimum-energy structure, and its production by ESI, could be favored both kinetically and thermodynamically. According to our computations, the *N*-protomer must surmount a barrier of 58.45 kcal/mol to isomerize into the *para*-protomer (Figure 3, TS1-3). Thus, the local activation ("heating") afforded the ion by acceleration and collisions while it is passing through the sampling cone region can provide the energy required for the transformation. Once a proton from the protonated amino group is transferred to the *ortho*-ring carbon via the four-member transition state TS1-3, it can migrate onto the other ring positions (**3** and **4**; Figure 3) with relative ease and end up forming the *para*-protomer (**5**; Figure 3) [28]. The observation that the *ring*-protomer is more prone to unimolecular fragmentations in the trap region than the *N*-protomer (Figure 1b) supports the notion that tautomerization occurs in the sampling-cone region and the *ring*-protomer accrues more energy than the *N*-protomer while passing through this region. For example, the MS^2 spectra recorded at low collision energy (not sufficient to instigate collisional activation) from the *ring*-protomers generated at low cone voltage (10–60 V) showed the base peak at *m/z* 94 (Figure 4a 1–6). In

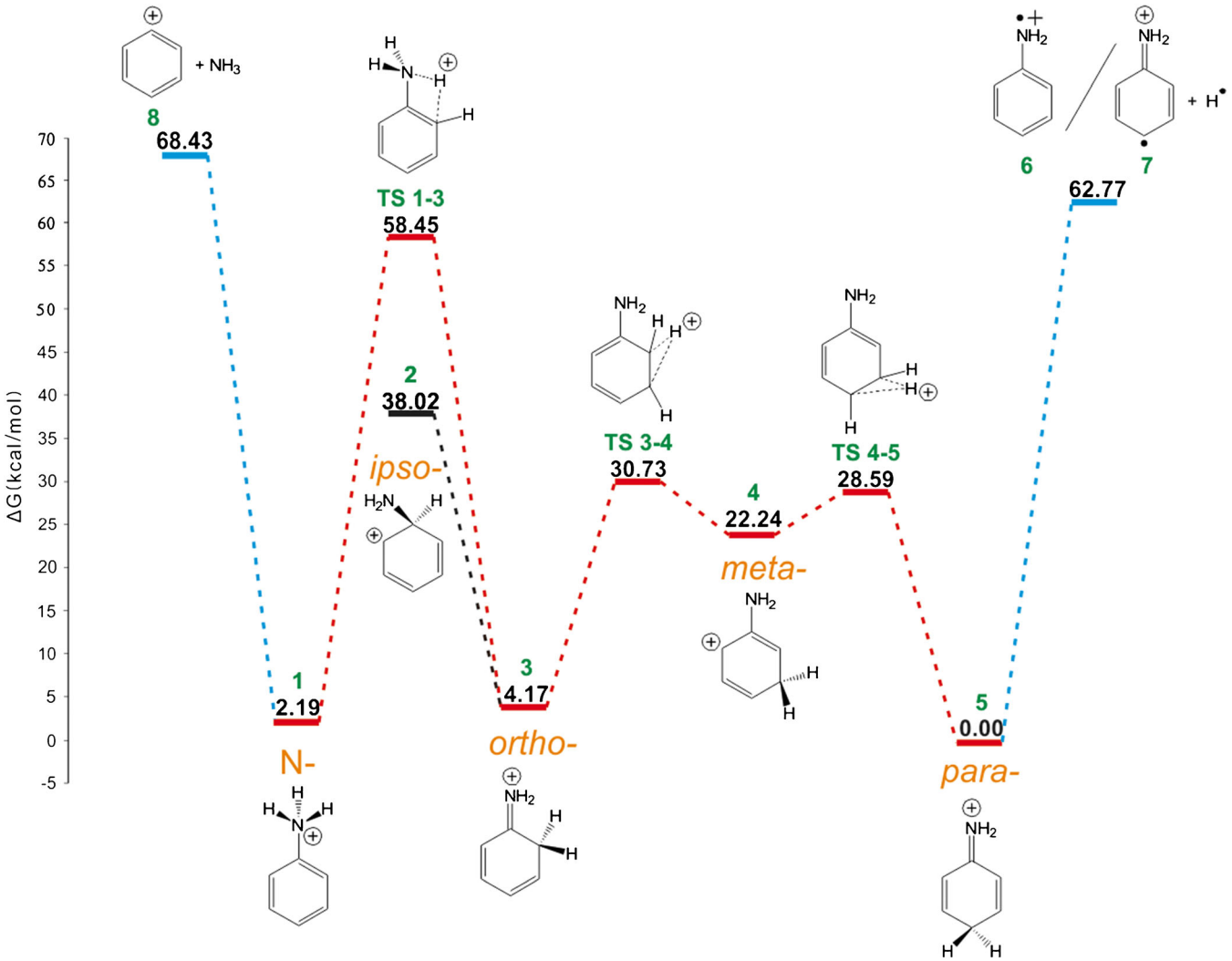

Figure 3. Relative Gibbs free energies [in kcal/mol, computed for 298.15 K and 1 atm by the density functional theory method B3LYP using a 6-311++G(2d,2p) basis set] and structures of energy-optimized ions, transition states, and products associated with the dissociation of *N*-protonated aniline

contrast, the *ring*-protomers generated at high cone voltage (80–100 V) arrive sufficiently energized to undergo unimolecular fragmentations after mass selection, to manifest the base peak at *m/z* 93 (Figure 4a 8–10).

Moreover, it is interesting to note that the peak for the *m/z* 77 ion (**8**) can be seen in the product-ion spectra of the *m/z* 94 ion only when the Trap and Transfer CID gas is present (Supplementary Figure S3). This observation suggests not only that the formation of the *m/z* 77 ion from the *N*-protomer requires an additional internal-energy increase in the precursor ion by collisional activation but also that the *C*-protomer re-tautomerizes to a certain extent upon encountering argon in the collision cells. This notion is supported by the observation of the *m/z* 77 peak in the CID spectrum of the mobility-separated *C*-protomer (Supplementary Figure S4). If the *C*-protomer re-tautomerizes to the *N*-protomer upon collision, the product-ion spectra recorded by increasing the Transfer-cell collision energy do not necessarily represent the bona fide fragmentation pattern of an *individual* mobility-separated protomer. Evidently, the afore-recognized post-ionization isomerization process is not a phenomenon unique to aniline [40]. The tautomerization process, in fact, recalls the *mobile proton model* proposed for peptides, which states that the proton initially localized on the most basic site of a molecule can be transferred to other sites upon activation [50]. Consequently, a heterogeneous population of protonated forms can be generated from a single analyte [51]. We obtained similar in-source tautomerization results from several other aromatic amines. For example, the protomer populations of *p*-toluidine are also dramatically affected by changes to the cone voltage. The arrival-time profile recorded from the selected *m/z* 108 $(M + H)^+$ ion from *p*-toluidine, generated at a sampling-cone voltage of 30 V, showed essentially only one peak, which represented the less mobile *N*-protomer (Figure 5a). As the cone voltage was raised, a second peak for the *C*-protomer appeared in the ARD profile (Figure 5b). At a cone voltage of 70 V, an intensity ratio of 2:3 was achieved for the 6.24 and 7.28 ms arrival-time peaks (Figure 5b). The mass spectra recorded from the two IM-separated protomers (Figure 5b1 and b2) under minimal CID conditions (Trap

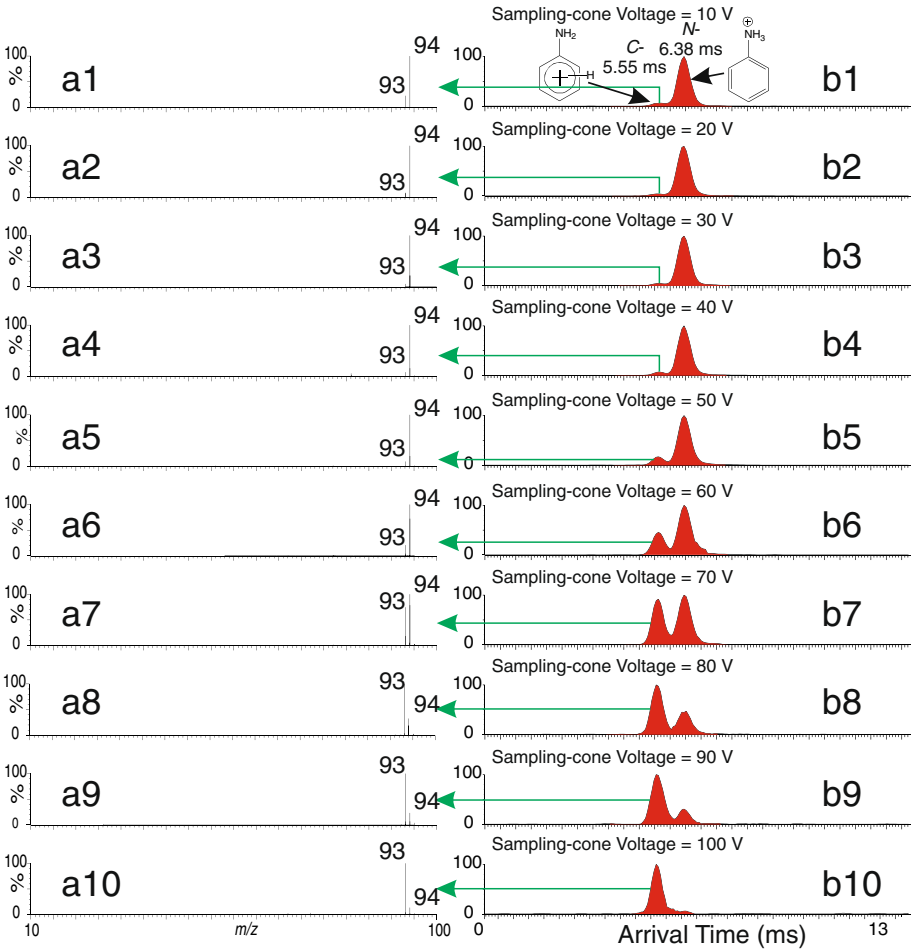

Figure 4. Arrival-time profiles recorded from the mass-selected *m/z* 94 ion generated by ESI from aniline (B1-B10), and CID spectra corresponding to the 5.55 ms peak for the *C*-protomer of aniline (A1-10). Spectra (*m/z* 10–1500) were recorded at sampling-cone voltage settings of 10, 20, 30, 40, 50, 60, 70, 80, 90, and 100 V on a Synapt G2 HDMS instrument. Ions were generated by ESI at a Vernier-probe-adjuster setting of 5.92 mm by spraying an aqueous sample of aniline. The mass-selected *m/z* 94 ions were separated by ion mobility at an IM wave velocity of 1500 m/s and a wave height 40.0 V. The capillary voltage was set to 2.55 kV, extraction cone 3.0 V, and desolvation-gas flow rate 477 L/h. The source- and desolvation-gas temperatures were held at 80 and 100 °C, respectively. The Trap collision energy was set to 4 eV and the Transfer collision energy to 2 eV

and Transfer collision energies 4 eV and 2 eV, respectively) confirmed that little or no fragmentation of the *m/z* 108 ion takes place in the Triwave region. However, when the transfer collision energy was increased to 20 eV, both protomers underwent facile fragmentation (Supplementary Figure S8). Upon activation, the *N*-protomer shows a near-equal tendency to eliminate either a $CH_3^{\bullet}$ or an NH_3 (Supplementary Figure S8B). In contrast, the activated *C*-protomer tends to lose a $CH_3^{\bullet}$ or a $H^{\bullet}$ (Supplementary Figure S8A). It has been argued that the differences in spectra acquired under different in-source ion-activation conditions can be rationalized by assuming that the protomer abundance ratio generated in the ion source is intrinsic, but that the fragmentation rates of the two are significantly different [10, 33]. However, our spectra recorded from *p*-toluidine clearly demonstrate that the intensity increase of the 6.24 ms peak is *not* due to differences in the fragmentation rates of the two protomers. Up to a sampling-cone voltage setting of 30 V, only peaks for the *N*-protomer were observed in the arrival-time profiles. As the cone voltage was gradually increased to 70 V, the rate of tautomerization and relative population of the *para*-protonated species also increased (Figure 5b).

Ab initio calculations suggested that the preferred protonation site of *p*-toluidine is the nitrogen atom (Supplementary Figure S9). This result is congruent with our experimental observation that at low sampling-cone voltages, only one peak appeared in the arrival-time profile (Figure 5a). The structure of the slower-moving protomer that corresponded to the 7.28 ms peak was confirmed by the post-IM mass spectrum recorded at a Transfer collision energy of 20 eV. The product-ion spectrum obtained showed an intense fragment-ion peak at *m/z* 91 attributable to an ammonia loss from the precursor ion (Supplementary Figure S8 B1). In contrast, the product-ion spectrum recorded from the faster-moving protomer, for which a mobility peak appeared only when the sampling-cone voltage was raised above 35 V, showed intense peaks at *m/z* 107 and 106 for

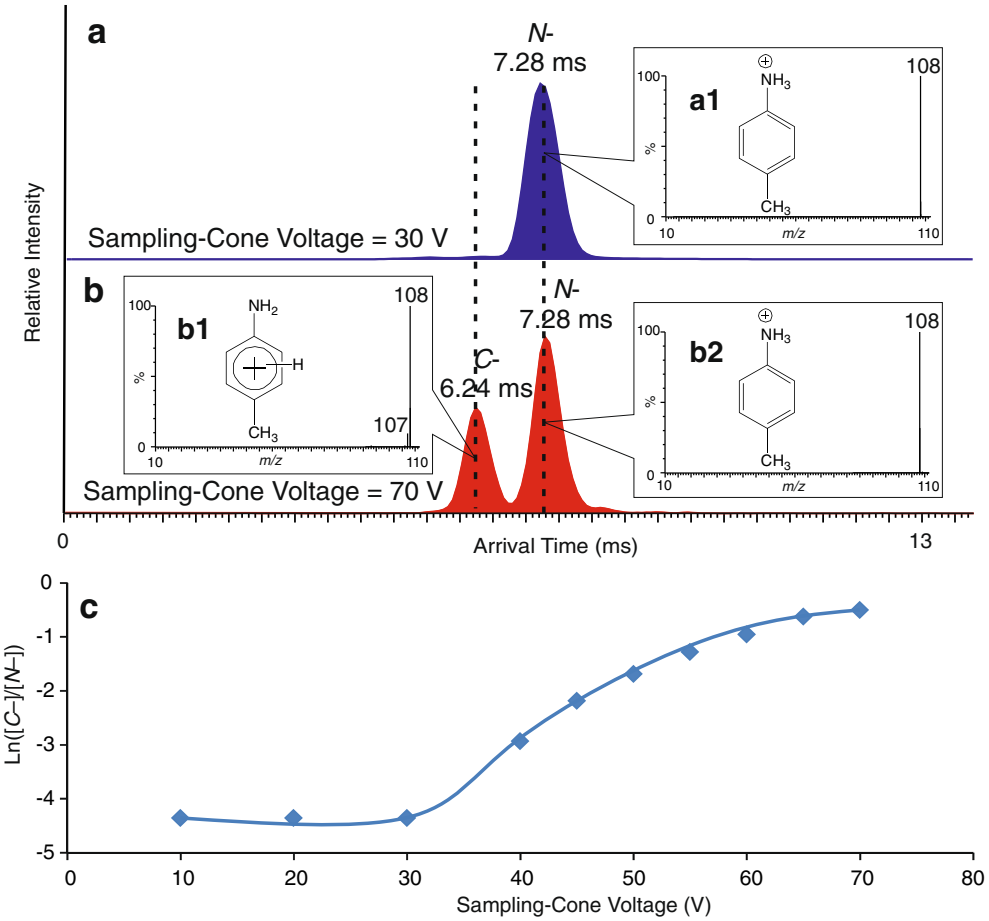

Figure 5. Arrival-time distributions recorded from the mass-selected *m/z* 108 ion generated from aqueous *p*-toluidine by ESI at a sampling-cone voltage of 30 V (**a**), and 70 V (**b**), recorded on a Synapt G2 HDMS instrument by ion-mobility separation, at an IMS wave velocity of 1500 m/s and a wave height 40.0 V. Ions were generated by HePI at a Vernier-probe-adjuster setting of 5.92 mm by placing samples near the cone and capillary tip within the ion-source chamber. The capillary voltage was set to 3.67 kV, the extraction cone at 3.0 V, desolvation-gas flow rate at 477 L/h, and HePI-gas flow rate at 30 mL/min (He). Insets A1 and B2 show CID spectra corresponding to the ARD peak at 7.28 ms, and Inset B1 shows that for the 6.24 ms peak. Panel (**c**) shows a plot of the natural logarithm of *C*-/*N*- peak intensity ratios extracted from arrival-time distributions recorded at different cone voltages

the respective $H^{\bullet}$ and H_2 losses from the precursor ion (Supplementary Figure S8 A1). Presumably, the formation of 4-methylenecyclohexa-2,5-dien-1-iminium cation is the driving force for this H_2 elimination (Supplementary Scheme S1). This result confirmed that the peak with an arrival time of 6.24 ms represents the *C*-protonated *p*-toluidine. According to our computations, the protonation on the *ortho*-ring carbon is only slightly less favored than the formation of the *N*-protomer (Supplementary Figure S9). The in-source ion activation provides the energy required to surmount the barrier for the isomerization of the *N*-protomer to the *C*-protomer via a proton migration.

Analogous experiments conducted with *p*-aminophenol and *p*-fluoroaniline showed that the protomer ratios of these compounds are also significantly influenced by the cone-voltage settings (Figure 6). For example, at a sampling-cone setting of 30 V, the ARP recorded for protonated *p*-aminophenol showed essentially one peak for the *N*-protomer (Figure 6a). As the cone voltage was raised, a new peak appeared at 6.24 ms for the *C*-protomer. The *C*-protomer produced in this way is very fragile and undergoes a rapid $H^{\bullet}$ loss, even faster than that observed from the *C*-protomer of aniline. Interestingly, the Transfer-CID spectra recorded from the *C*-protomer showed a peak at *m/z* 111 (Supplementary Figure S10 A1). Because the *m/z* 111 ion is generated after the mass-selection of the *m/z* 110 ion, it was evident that this enigmatic ion must originate from an ion-molecule adduct formation reaction that took place in the collision cell. The rationalization is that the water present as an impurity in the Transfer collision gas (although the gas used was the highest quality dry argon, which manufacturers label "bone dry") adds to the *m/z* 93 ion (which originates by an ammonia loss from the *m/z* 110 ion (Supplementary Figure S10) to generate the *m/z* 111 ion (water and other neutral-molecule additions to ions in the mobility and collision cells have been noted previously [28, 52]). In contrast, the *m/z* 93 ion generated from the *N*-protomer produced only negligible traces of the water adduct under identical experimental conditions (Supplementary

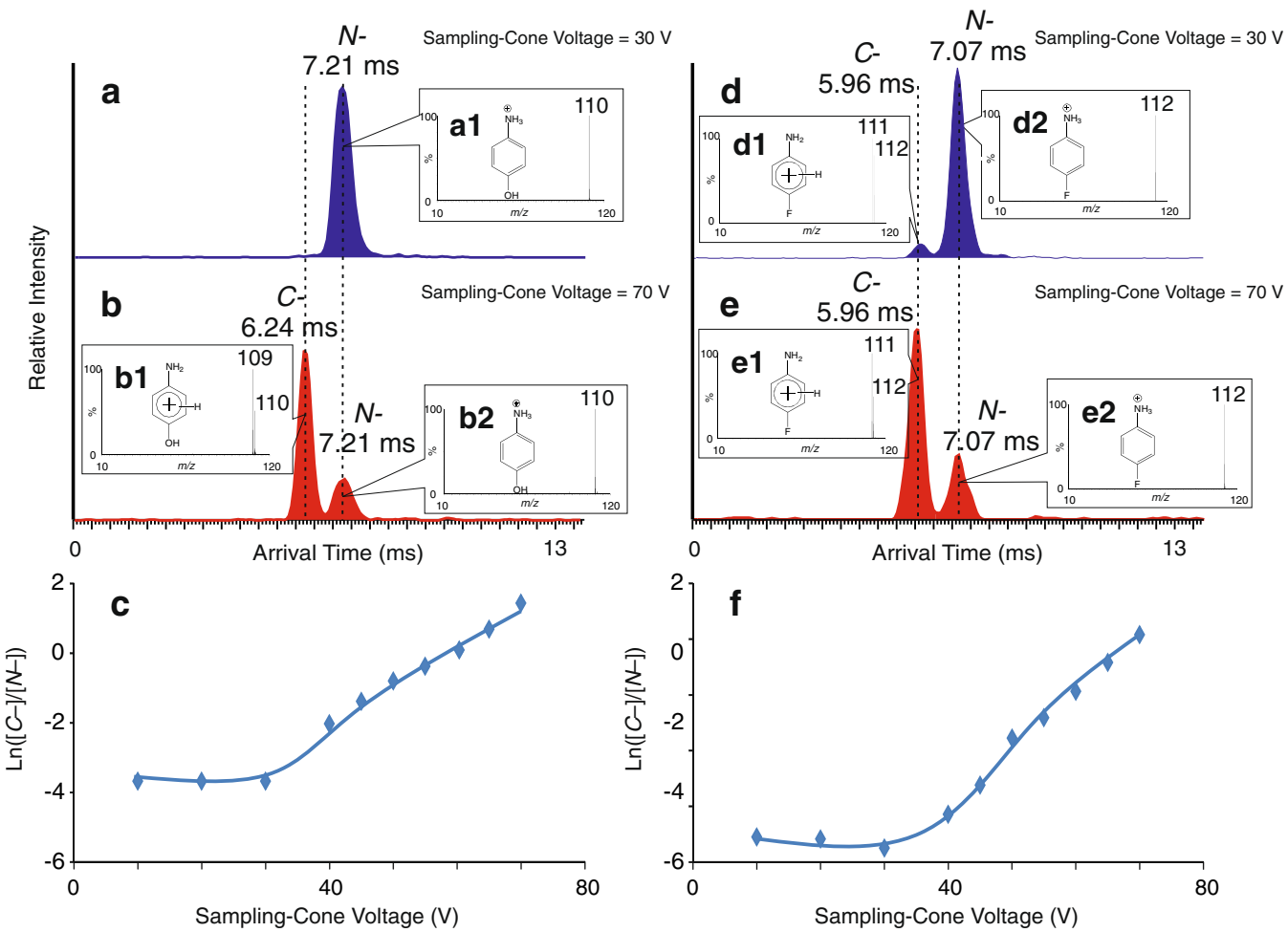

Figure 6. Arrival-time distributions recorded from mass-selected *m/z* 110 and 112 ions generated from *p*-aminophenol and *p*-fluoroaniline, respectively, at sampling-cone voltages of 30 (**a** and **d**) and 70 V (**b** and **e**), recorded on a Synapt G2 HDMS instrument by ion-mobility separation at an IM wave velocity of 1500 m/s and a wave height 40.0 V. Ions were generated by HePI at a Vernier-probe-adjuster setting of 5.92 mm by placing samples near the cone and capillary tip within the ion-source chamber. The capillary voltage was set to 3.67 kV, extraction cone at 3.0 V, desolvation-gas flow rate at 477 L/h, and HePI-gas flow rate at 30 mL/min (He). Insets A1 and B2 show CID spectra corresponding to the ARD peak at an arrival time of 7.21 ms, and the inset B1 shows that for the 6.24 ms peak. Similarly, insets D1 and E1 show spectra for 5.96 ms, and insets D2 and E2 show spectra for 7.07 ms ARD peaks recorded from *p*-fluoroaniline. Panels (**c**) and (**f**) show plots of the natural logarithm of *C*-/*N*- peak intensity ratios extracted from data recorded at different sampling cone voltage settings, from *p*-aminophenol and *p*-fluoroaniline, respectively

Figure S10 B). Initially, the result was puzzling because the *m/z* 93 ion is expected to be generated only from the *N*-protomer by an NH_3 loss. Similar to the observations made with *ring*-protonated aniline, the *C*-protomer of *p*-aminophenol re-tautomerizes to the *N*-protonated species upon collisions in the transfer cell, and the latter ion subsequently loses NH_3 to generate the *m/z* 93 ion. The *m/z* 93 ion generated in this way is relatively less activated (a "cool" ion), and hence it is now able to react with water in the collision gas, whereas the *m/z* 93 ion generated directly from the *N*-protomer is too energetic ("hot") to do so.

Experiments conducted with protonated *p*-fluoroaniline also showed that its *N*-protomer predominates at low cone voltages. As the cone voltage is raised (Figure 6e), the population of the *C*-protomer increases. The Transfer-CID spectra recorded at 20 eV from the *N*-protomer demonstrated that it loses NH_3 and HF (Supplementary Figure S11 B1), whereas the *C*-protomer loses a $H^{\bullet}$ (Supplementary Figure S11 A1). The presence of a peak at *m/z* 95 in the spectrum of the *C*-protomer indicated that the *C*-protomer re-tautomerizes to a small extent to the *N*-protomer upon activation (Supplementary Figure S11 A1).

Conclusions

Flammang et al. [28] noted that ESI mass spectra of aniline recorded at three different cone voltages were different, and recognized the significance of the co-occurrence of its *N*- and *C*-protomers. Owing to the different proportions of protomers

that could be present at different cone-voltage settings, such dissimilarities are expected. The solvent composition and the pH of the solution have been considered to be the most important factors determining protomer abundance ratios for aromatic compounds under ESI conditions [53]. However, our results demonstrate that ESI *instrumental* parameters also exert dramatic effects on the abundances of different protomers generated from the same compound. We have shown that the protomer ratio is affected by the cone voltage regardless of whether the ions are generated by ESI or by plasma ionization of analytes after direct thermal desorption from neat liquids or solid residues without the intervention of a solvent.

For identification and characterization of drugs and their metabolites by mass spectrometry, it is important to develop reliable interpretation rules. Although enormous research efforts have been focused in this direction, nearly all attempts to interpret fragmentation spectra begin by preselecting and assigning one specific structure to represent the precursor ion. The results reported herein indicate that most of the interpretation mechanisms proposed on the basis of composite spectra must be improved by considering the fact that an activated protomer or, respectively, a deprotomer in the negative ionization mode, can exist in multiple tautomeric forms. The exact structural nature of a precursor ion must be correctly recognized before a rational fragmentation mechanism is proposed. However, establishing an unambiguous precursor structure for activated ions is not an easy task, particularly when the energy differences between the putative structures are small [25]. As we gather more information, it is becoming clearer that results based on solution chemistry and parameters such as gas-phase basicity cannot be used as sufficiently reliable criteria to predict fragmentation mechanisms of activated gaseous ions. Evidently, even for a simple ion such as protonated aniline, high-level theoretical methods are unable to provide unambiguous conclusions because structures proposed by computational energy-optimization methods are not very reliable for activated ions. Moreover, an extensive study carried out by Russo et al. to determine the preferred protonation site of aniline in the gas phase by computing the energetic parameters at many different levels of theory and the DFT-based reactivity descriptors demonstrated that energy values predicted by various methods can sometimes differ by up to 10 kcal/mol [25]. Some library mass spectra are listed from data collected without the appreciation of the fact that the initial precursor-ion structures may be composites. Thus, CID libraries should be used with caution for computer-based identification of compounds.

References

1. Pollack, S.K., Devlin III, J.L., Summerhays, K.D., Taft, R.W., Hehre, W.J.: The site of protonation in aniline. J. Am. Chem. Soc. **99**, 4583–4584 (1977)
2. Maquestiau, A., Van Haverbeke, Y., Mispreuve, H., Flammang, R., Harris, J.A., Howe, I., Beynon, J.H.: The gas-phase structure of some protonated and ethylated aromatic amines. Org. Mass Spectrom. **15**, 144–148 (1980)
3. McMahon, A.W., Chadikun, F., Harrison, A.G.: Site of protonation of aromatic compounds: A neutralization-reionization study. Int. J. Mass Spectrom. Ion Processes **87**, 275–285 (1989)
4. Lau, Y.K., Kebarle, P.: Substituent effects on the intrinsic basicity of benzene: proton affinities of substituted benzenes. J. Am. Chem. Soc. **98**, 7452–7453 (1976)
5. Karpas, Z., Berant, Z., Stimac, R.: An ion mobility spectrometry/mass spectrometry (IMS/MS) study of the site of protonation in anilines. Struct. Chem. **1**, 201–204 (1990)
6. Pachuta, S.J., Isern-Flecha, I., Cooks, R.G.: Charge stripping and the site of cationization of substituted aromatic compounds. Org. Mass Spectrom. **21**, 1–5 (1986)
7. Harrison, A.G.: Site of gas-phase ethyl ion attachment. Can. J. Chem. **64**, 1051–1053 (1986)
8. Smith, R.L., Chyall, L.J., Beasley, B.J., Kenttämaa, H.I.: The site of protonation of aniline. J. Am. Chem. Soc. **117**, 7971–7973 (1995)
9. Nold, M.J., Wesdemiotis, C.: Differentiation of N- from C-protonated aniline by neutralization-reionization. J. Mass Spectrom. **31**, 1169–1172 (1996)
10. Wang, J., Aubry, A., Bolgar, M.S., Gu, H., Olah, T.V., Arnold, M., Jemal, M.: Effect of mobile phase pH, aqueous-organic ratio, and buffer concentration on electrospray ionization tandem mass spectrometric fragmentation patterns: implications in liquid chromatography/tandem mass spectrometric bioanalysis. Rapid Commun. Mass Spectrom. **24**, 3221–3229 (2010)
11. Lee, S.-W., Cox, H., Goddard III, W.A., Beauchamp, J.L.: Chemistry in nanodroplets: studies of protonation sites of substituted anilines in water clusters using FT-ICR. J. Am. Chem. Soc. **122**, 9201–9205 (2000)
12. Lau, Y.K., Nishizawa, K., Tse, A., Brown, R.S., Kebarle, P.: Protonation and site of protonation of anilines. Hydration and site of protonation after hydration. J. Am. Chem. Soc. **103**, 6291–6295 (1981)
13. Albert, A., Shelley, J.T., Engelhard, C.: Plasma-based ambient desorption/ionization mass spectrometry: state-of-the-art in qualitative and quantitative analysis. Anal. Bioanal Chem **406**, 6111–6127 (2014)
14. Taylor, P. J., van der Zwan, G., Antonov, L.: Tautomerism: methods and theories, pp. 1–24. Wiley-VCH: Weinheim, Germany (2014)
15. Chetverin, A.B.: Evidence for a diprotomeric structure of Na, K-ATPase: accurate determination of protein concentration and quantitative end-group analysis. FEBS Lett. **196**, 121–125 (1986)
16. Tian, Z., Kass, S.R.: Gas-Phase versus liquid-Phase structures by electrospray ionization mass spectrometry. Angew. Chem. Int. Ed. **48**, 1321–1323 (2009)
17. Schmidt, J., Meyer, M.M., Spector, I., Kass, S.R.: Infrared multiphoton dissociation spectroscopy study of protonated *p*-aminobenzoic acid: does electrospray ionization afford the amino- or carboxy-protonated ion? J. Phys. Chem. A **115**, 7625–7632 (2011)
18. Chai, Y., Hu, N., Pan, Y.: Kinetic and thermodynamic control of protonation in atmospheric pressure chemical ionization. J. Am. Soc. Mass Spectrom. **24**, 1097–1101 (2013)
19. Campbell, J.L., Yves Le Blanc, J.C., Schneider, B.B.: Probing electrospray ionization dynamics using differential mobility spectrometry: the curious case of 4-aminobenzoic acid. Anal. Chem. **84**, 7857–7864 (2012)
20. Chang, T.M., Prell, J.S., Warrick, E.R., Williams, E.R.: Where's the charge? Protonation sites in gaseous ions change with hydration. J. Am. Chem. Soc. **134**, 15805–15813 (2012)
21. Campbell, J.L., Yang, A.M.-C., Melo, L.R., Hopkins, W.S.: Studying gas-phase interconversion of tautomers using differential mobility spectrometry. J. Am. Soc. Mass Spectrom. **27**, 1277–1284 (2016)
22. Ritchie, J.P.: Some comments concerning the use of static charge distributions for predicting chemical reactivity. J. Mol. Struct. Theochem. **255**, 297–308 (1992)
23. Hillebrand, C., Klessinger, M., Eckert-Maksic, M., Maksic, Z.B.: Theoretical model calculations of the proton affinities of aminoalkanes, aniline, and pyridine. J. Phys. Chem. **100**, 9698–9702 (1996)
24. Roy, R.K., de Proft, F., Geerlings, P.: Site of protonation in aniline and substituted anilines in the gas phase: a study via the local hard and soft acids and bases concept. J. Phys. Chem. A **102**, 7035–7040 (1998)
25. Russo, N., Toscano, M., Grand, A., Mineva, T.: Proton affinity and protonation sites of aniline. Energetic behavior and density functional reactivity indices. J. Phys. Chem. A **104**, 4017–4021 (2000)
26. Bagno, A., Terrier, F.: Carbon and nitrogen basicity of aminothiophenes and anilines. J. Phys. Chem. A **105**, 6537 (2001)

27. Chyall, L.J., Kenttämaa, H.I.: The 4-dehydroanilinium ion: a stable distonic isomer of ionized aniline. J. Am. Chem. Soc. **116**, 3135–3136 (1994)
28. Flammang, R., Dechamps, N., Pascal, L., Haverbeke, Y.V., Gerbaux, P., Nam, P., Nguyen, M.T.: Ring versus nitrogen protonation of anilines. Lett. Org. Chem. **1**, 23–30 (2004)
29. Joyce, J.R., Richards, D.S.: Kinetic control of protonation in electrospray ionization. J. Am. Soc. Mass Spectrom. **22**, 360–368 (2011)
30. Lapthorn, C., Dines, T.J., Chowdhry, B.Z., Perkins, G.L., Pullen, F.S.: Can ion mobility mass spectrometry and density functional theory help elucidate protonation sites in 'small' molecules? Rapid Commun. Mass Spectrom. **27**, 2399–2410 (2013)
31. Ranasinghe, Y.A., Glish, G.L.: Reactions of the phenylium cation with small oxygen- and nitrogen-containing molecules. J. Am Soc. Mass Spectrom. **7**, 473–481 (1996)
32. Bakhtiar, R., Holznagel, C.M., Jacobson, D.B.: Efficient isomerization of Si (C2H5) H2+ to Si (CH3) 2H+ by collisional activation in the gas phase. Organometallics **12**, 621–623 (1993)
33. Kaufmann, A., Butcher, P., Maden, K., Widmer, M., Giles, K., Uría, D.: Are liquid chromatography/electrospray tandem quadrupole fragmentation ratios unequivocal confirmation criteria? Rapid Commun. Mass Spectrom. **23**, 985–998 (2009)
34. Kovačević, B., Schorr, P., Qi, Y., Volmer, D.A.: Decay mechanisms of protonated 4-quinolone antibiotics after electrospray ionization and ion activation. J. Am. Soc. Mass Spectrom. **25**, 1974–1986 (2014)
35. Giles, K., Williams, J.P., Campuzano, I.: Enhancements in traveling wave ion mobility resolution. Rapid Commun. Mass Spectrom. **25**, 1559–1566 (2011)
36. Hunt, S.M., Sheil, M.M., Belov, M., Derrick, P.J.: Probing the effects of cone potential in the electrospray ion source: consequences for the determination of molecular weight distributions of synthetic polymers. Anal. Chem. **70**, 1812–1822 (1998)
37. Klagkou, K., Pullen, F., Harrison, M., Organ, A., Firth, A., Langley, G.J.: Approaches towards the automated interpretation and prediction of electrospray tandem mass spectra of non-peptidic combinatorial compounds. Rapid Commun. Mass Spectrom. **17**, 1163–1168 (2003)
38. Venkataraghavan, R., McLafferty, F.W., van Lear, G.E.: Computer-aided interpretation of mass spectra. Org. Mass Spectrom. **2**, 1–15 (1969)
39. Révész, A., Schröder, D., Rokob, T.A., Havlik, M., Dolenský, B.: Identification and interconversion of diastereomeric oligo-Tröger bases probed by ion mobility mass spectrometry. Phys. Chem., Chem. Phys. **14**, 6987–6995 (2012)
40. Xia, H., Attygalle, A.B.: Effect of electrospray ionization source conditions on tautomer distribution of deprotonated *p*-hydroxybenzoic acid in gas phase. Anal. Chem. **88**, 6035–6043 (2016)
41. Yang, Z., Pavlov, J., Attygalle, A.B.: Quantification and remote detection of nitro explosives by helium plasma ionization mass spectrometry (HePI-MS) on a modified atmospheric pressure source designed for electrospray ionization. J. Mass Spectrom. **47**, 845–852 (2012)
42. Frisch, M. J., Trucks, G.W., Schlegel, H.B., Scuseria, G.E., Robb, MA., Cheeseman, J. R., Scalmani, G., Barone, V., Mennucci, B., Petersson, G.A., Nakatsuji, H., Caricato, M., Li, X., Hratchian, H.P., Izmaylov, A.F., Bloino, J., Zheng, G., Sonnenberg, J.L., Hada, M., Ehara, M., Toyota, K., Fukuda, R., Hasegawa, J., Ishida, M., Nakajima, T., Honda, Y., Kitao, O., Nakai, H., Vreven, T., Montgomery, J.A. Jr., Peralta, E., Ogliaro, F., Bearpark, M., Heyd, J.J., Brothers, E., Kudin, K.N., Staroverov, V.N., Keith, T., Kobayashi, R., Normand, J., Raghavachari, K., Rendell, A., Burant, J.C., Iyengar, S.S., Tomasi, J., Cossi, M., Rega, N., Millam, J.M., Klene, M., Knox, J.E., Cross, J.B., Bakken, V., Adamo, C., Jaramillo, J., Gomperts, R., Stratmann, R.E., Yazyev, O., Austin, A.J., Cammi, R., Pomelli, C., Ochterski, J.W., Martin, R.L., Morokuma, K., Zakrzewski, V.G., Voth, G.A., Salvador, P., Dannenberg, J.J., Dapprich, S., Daniels, A.D., Farkas, O., Foresman, J.B., Ortiz, J.V., Cioslowski, J., Fox, D.J.: Gaussian 09, rev. B.01; Gaussian, Inc.: Wallingford CT (2010)
43. Becke, A.D.: Density-functional thermochemistry. III. The role of exact exchange. J. Chem. Phys. **98**, 5648–5652 (1993)
44. Lee, C., Yang, W., Parr, R.G.: Phys. Rev. B **37**, 785–789 (1988)
45. Pertel, R.: Molecular beam sampling of dynamic systems. Int. J. Mass Spectrom. Ion Process **16**, 39–52 (1975)
46. Katta, V., Chowdhury, S.K., Chait, B.T.: Use of a single-quadrupole mass spectrometer for collision-induced dissociation studies of multiply charged peptide ions produced by electrospray ionization. Anal. Chem. **63**, 174–178 (1991)
47. Voyksner, R.D., Pack, T.: Investigation of collisional-activation decomposition process and spectra in the transport regions of an electrospray single-quadrupole mass spectrometer. Rapid Commun. Mass Spectrom. **5**, 263–268 (1991)
48. Lalli, P.M., Iglesias, B.A., Toma, H.E., de Sa, G.F., Daroda, R.J., Silva Filho, J.C., Szulejko, J.E., Araki, K., Eberlin, M.N.: Protomers: formation, separation, and characterization via traveling wave ion mobility mass spectrometry. J. Mass Spectrom. **47**, 712–719 (2012)
49. McEwen, C.N., McKay, R.G., Larsen, B.S.: Analysis of solids, liquids, and biological tissues using solids probe introduction at atmospheric pressure on commercial LC/MS instruments. Anal. Chem. **77**, 7826–7831 (2005)
50. Boyd, R., Somogyi, Á.: The mobile proton hypothesis in fragmentation of protonated peptides: a perspective. J. Am. Soc. Mass Spectrom. **21**, 1275–1278 (2010)
51. Wysocki, V.H., Tsaprailis, G., Smith, L.L., Breci, L.A.: Mobile and localized protons: a framework for understanding peptide dissociation. J. Mass Spectrom. **35**, 1399–1406 (2000)
52. Schröder, D.: Ion-mobility mass spectrometry of complexes of nickel and acetonitrile. Collect. Czech. Chem. Commun. **76**, 351–369 (2011)
53. Warnke, S., Seo, J., Boschmans, J., Sobott, F., Scrivens, J.H., Bleiholder, C., Bowers, M.T., Gewinner, S., Schöllkopf, W., Pagel, K., von Helden, G.: Protomers of benzocaine: solvent and permittivity dependence. J. Am. Chem. Soc. **137**, 4236–4242 (2015)